Aqua Slide: An Underwater Leveling Motion Scheme for M-UAAV Utilizing Singularity

Dongyue Huang ©, *Graduate Student Member, IEEE*, Minghao Dou ©, Xuchen Liu ©, Xinyi Wang ©, Chenggang Wang ©, and Ben M. Chen ©, *Fellow, IEEE*

Abstract—The underwater leveling motion control of a morphable unmanned aerial–aquatic vehicle (M-UAAV) is essential but lacks an elegant solution. In this article, a scheme named Aqua Slide is proposed for Mirs-Alioth, our predeveloped M-UAAV prototype, to achieve underwater leveling motions by utilizing singularity. For the first time, the singular thrust tilt angle (STTA), i.e., the tilt angle that causes a vehicle to reach singularity, is characterized and defined. For underwater leveling motion generation, STTA is utilized as a key tool. Crucial factors of these motions, i.e., the existence of control direction uncertainty, and coupling effects are identified. Aqua Slide is proposed to tackle the crucial factors in generating underwater leveling motions, consisting of an STTA controller, a primary-auxiliary switch, and an auxiliary controller incorporating the saturated Nussbaum function. A simulation environment, enriched with a detailed model, is established using a Gazebo and hardware-in-the-loop (HITL) configuration. Under similar control parameter settings, full-cycle Gazebo-HITL simulations and experiments reveal the effectiveness of the approach. The vehicle maintains the attitude within a maximum of 5° during the whole procedure. Meanwhile, the ablation studies in Aqua Slide highlight the indispensability of the submodules in the approach. The absence of any module results in undesirable or even divergent behavior of Mirs-Alioth during underwater leveling motions. The preliminary exploration in this article elegantly solves the issue of generating underwater leveling motion for an M-UAAV and provides a referential solution for transitioning from simulation to real-world applications. Video attachment: https://youtu.be/XpViXL0qcvk.

Index Terms—Attitude control, marine vehicles, morphable unmanned aerial–aquatic vehicles (M-UAAVs), unmanned aerial vehicles (UAVs).

I. INTRODUCTION

VARIOUS unmanned aerial–aquatic vehicles (UAAVs) are developed for accomplishing aerial and aquatic multi-disciplinary tasks to alleviate human labor [1], [2]. Due to the structural characteristics of UAAVs, they hold significant potential for various industrial applications, such as 3-D cross-domain networking and heterogeneous multimarine robot collaboration [3], [4]. This has led to increasing attention in UAAVs. Compared with the fixedly tilted rotors UAAVs like [5], [6], [7], a series of morphable UAAVs (M-UAAVs) are proposed to improve maneuverability for underwater locomotion. For example, [8] is an over-actuated M-UAAV, [9] has no underwater maneuverability, and [10], [11] are M-UAAVs with one side of rotor tiltable. Differently, to guarantee a proper weight for aerial flight, we developed an under-actuated M-UAAV, referred to as "Mirs-Alioth" [12]. It has a tiltable component to change all rotors' direction in a coupling mechanically-linked manner [13], as shown in Fig. 1. Detailed mechanical descriptions are found in [14].

Leveling motion is crucial and necessary in industrial tasks such as inspection and tracking involving UAAVs. Because large attitude changes can disrupt onboard sensors like cameras. This leads to issues such as motion blur or ego-motion failure, which complicates exploration and monitoring efforts [15]. The leveling motion allows the vehicle operate movement keeping the attitude level, as shown in Fig. 1. Tan and Chen have roughly and briefly pointed out specific thrust tilt angles that result in no torque acting on the fuselage, leading solely to translation in Mirs-Alioth [16]. Since these cases meet the definition of singularity in robotics [17], these configurations are referred to as singularities. The thrust tilt angle causing singularity is termed the singular thrust tilt angle (STTA), which serves as a key tool for generating underwater leveling motion.

Many studies focus on achieving the leveling motion of similar robotics to Mirs-Alioth. To our knowledge, the only research achieving leveling motion in an under-actuated M-UAAV prototype is [10], and in an under-actuated underwater robot, [18].
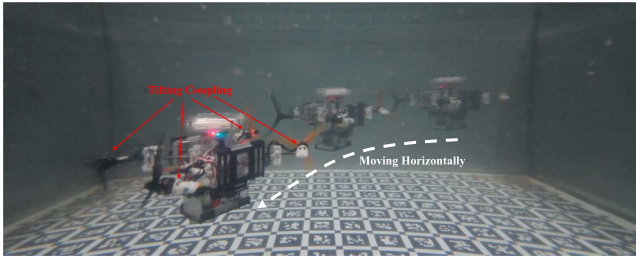
Fig. 1. Snapshot of the prototype M-UAAV with the coupling tilting mechanism: Mirs-Alioth operating in underwater leveling motion.

Fig. 2. Mirs-Alioth. (a) Snapshot of the prototype working underwater. (b) Rendering CAD model in the Gazebo-HITL simulation.

The former used simpler fixed tilt angles corresponding to different modes, while the latter employed switching control between predefined fixed thrust angles. The lack of continuous tilt control leads to reduced actuation efficiency, increased vibration, and sometimes divergence. On the other hand, some studies have successfully achieved leveling motion in underactuated tilt tri-rotor UAVs using adaptive control [19] and modified sliding mode control [20]. However, two key differences in their locomotion design limit their applicability to Mirs-Alioth. First, the operating environments and configurations differ significantly. Second, the tilting mechanisms vary across designs. For instance, [19] features two front rotors that tilt forward, while the rear rotor tilts laterally in [20], allowing these robots to perform leveling motions only in either forward or lateral directions, not both.

Therefore, a suitable approach to achieve the underwater leveling motions for Mirs-Alioth is necessary. Generally, singularity is avoided in fully/over-actuated tilt-rotor UAVs and tiltable underwater robotics due to the complications it introduces to the system [21]. Relevant references include [21], [22], [23], [24], [25] for UAVs and [18], [26], [27] for underwater robotics. On the contrary, for Mirs-Alioth, singularity is leveraged as a beneficial feature. As an under-actuated system, it cannot completely decouple linear and angular motions. Yet, the singularity allows angular motion to be isolated from linear motion at certain thrust tilt angles. Additionally, the buoyancy alleviates the burden of thrust in the vertical direction. Integrating the above factors makes such motions feasible. Consequently, a controller that ensures the thrust tilt angle lies within the STTA, leveraging its singularity property to prevent angular motion generated by operating on the fuselage, is designed to generate the described motions.

However, utilizing the above controller exclusively leads to challenges. For example, the coupling-tilting mechanism permits underwater leveling motion in forward and lateral directions but increases control complexity, such as control directional uncertainty and coupling effects. To the best of our knowledge, this article is the first to raise the issue of control directional uncertainty in the control of UAAVs. Therefore, this article proposes the integration of a Saturated Nussbaum function [28], [29] and an auxiliary controller to address these problems. These elements mitigate control directional uncertainty and coupling effects. Furthermore, the controller is designed under a switching-based framework
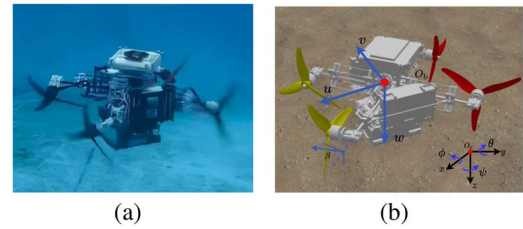
[30], allowing for efficient transitions between forward and lateral motions.

To this end, this article proposes a novel scheme by singularity for M-UAAV to achieve underwater leveling motions. The scheme, named Aqua Slide, is developed, simulated, and experimentally validated to generate underwater leveling motions. Aqua Slide addresses crucial problems of underwater leveling motions for our prototype, Mirs-Alioth, by employing various sub-modules. These include handling variations in STTA between roll and pitch, managing uncertainty in the control direction, and mitigating the coupling effect. Mirs-Alioth achieves underwater leveling motions through its submodules, specifically the STTA controller for uni-directional leveling motion, the auxiliary controller and Nussbaum function to handle coupling and directional uncertainties during turns, and the switch to transition between forward and lateral locomotion. Simulations are conducted within a self-developed Gazebo-hardware-in-the-loop (HITL) framework, with physical experiments based on the same controller parameters. Cross-validation confirms that the proposed approach effectively enables an under-actuated M-UAAV to generate underwater leveling motions in forward or lateral directions. This article also conducts ablation studies to demonstrate the indispensability of sub-modules in managing control directional uncertainty and coupling effects.

The remainder of the article is organized as follows. Section II illustrates the mathematical model. Section III introduces the derivation of STTAs and analysis of underwater leveling motion based on STTA. Section IV introduces the details about Aqua Slide. Lastly, validations in the Gazebo-HITL simulation and experiment are conducted in Section V.

II. MATHEMATICAL MODEL

In this section, a fundamental model description of Mirs-Alioth is given, with decoupled motion models. Assuming the vehicle is fully submerged, Fig. 2(b) introduces two reference frames: the body reference frame (b-frame) affixed to the vehicle body with its origin at the center of buoyancy (CoB), denoted as O_b, and the inertial reference frame (e-frame) at O_e. Define $\boldsymbol{\nu} = [u\ v\ w\ p\ q\ r]^\mathrm{T}$ as the state, represented in the b-frame, the pose variable $\boldsymbol{\eta} = [x\ y\ z\ \phi\ \theta\ \psi]^\mathrm{T}$, both represented in e-frame, $\boldsymbol{J} = \mathrm{diag}([\boldsymbol{R}_\mathrm{b}^\mathrm{e}, \boldsymbol{S}^{-1}])$ is the transformation matrix [31].

Following what is proposed in [32], the mathematical model can be described as

$$\dot{\boldsymbol{\eta}} = \boldsymbol{J}\boldsymbol{\nu} \qquad (1)$$

$$\boldsymbol{M}\dot{\boldsymbol{\nu}} + \boldsymbol{C}(\boldsymbol{\nu})\boldsymbol{\nu} + \boldsymbol{D}\boldsymbol{\nu} + \boldsymbol{g}(\boldsymbol{\eta}) = \boldsymbol{\tau} + \boldsymbol{\tau}_\Delta \qquad (2)$$

where $\boldsymbol{M}$ is the inertial matrix, $\boldsymbol{C}(\boldsymbol{\nu})$ is the Coriolis and centripetal matrix, $\boldsymbol{D}$ is the damping matrix, and $\boldsymbol{g}(\boldsymbol{\eta})$ is the restoring force and moment vector. The elements $M_{ij}(i,j = 1, 2, \ldots, 6)$ in the inertial matrix include the rigid part parameters like the mass of the vehicle m and moment of inertial, such as I_{zz}. The added mass and inertial in hydrodynamics are also included and expressed as $X_{\dot{u}}$, $Y_{\dot{v}}$, $Z_{\dot{w}}$, $K_{\dot{p}}$, $M_{\dot{q}}$, and $N_{\dot{r}}$. The damping coefficients are defined as X_u, Y_v, Z_w, K_p, M_q, and N_r. More details are found from (30) to (36) of [33].

Besides, $\boldsymbol{\tau} = [\boldsymbol{F}_b \ \boldsymbol{M}_b]^T$ is the input vector of generalized force and moment, followed by $\boldsymbol{\tau} = \bar{\boldsymbol{B}}(\beta)\boldsymbol{u}$. In this context, both β and $\boldsymbol{u}$ serve as inputs in this system, with β adjusting the thrust tilt angle and $\boldsymbol{u}$ dictating the motor speeds. Specifically, β represents the symmetric thrust tilt angle, which varies from $-\pi/2$ to $\pi/2$, and is detailed in [16]. Additionally, the input vector is defined as $\boldsymbol{u} = \varpi_i^2$ ($i \in 1, 2, 3, 4$), where ϖ_i signifies the rotational speed of each of the four motors. And $\boldsymbol{\tau}_\Delta$ is the lumped vector including model uncertainty and external disturbances, followed by $\boldsymbol{\tau}_\Delta = \Delta \boldsymbol{B}\boldsymbol{u}$. Then the control effectiveness matrix (CEM) is as follows

$$\boldsymbol{B}(\beta) = \bar{\boldsymbol{B}}(\beta) + \Delta \boldsymbol{B} = \frac{\sqrt{2}}{2} \begin{bmatrix} (c_\beta K_T + \sqrt{2}\Delta_x) \cdot e_x \\ (c_\beta K_T + \sqrt{2}\Delta_y) \cdot e_y \\ -\sqrt{2}(s_\beta K_T - \Delta_z) \cdot e_z \\ (k_1(\beta) + \sqrt{2}\Delta_\phi) \cdot e_\phi \\ (k_2(\beta) + \sqrt{2}\Delta_\theta) \cdot e_\theta \\ \sqrt{2}(k_3(\beta) + \Delta_\psi) \cdot e_\psi \end{bmatrix} \qquad (3)$$

with

$$k_1(\beta) = l \cdot s_\beta \cdot K_T + c_\beta(K_M - z_t K_T) \qquad (4)$$
$$k_2(\beta) = -l \cdot s_\beta \cdot K_T + c_\beta(K_M + z_t K_T) \qquad (5)$$
$$k_3(\beta) = K_T l \cdot c_\beta - s_\beta \cdot K_M \qquad (6)$$

where $s_{(\cdot)}, c_{(\cdot)}, t_{(\cdot)}$ denote $\sin(\cdot)$, $\cos(\cdot)$, and $\tan(\cdot)$ respectively. Half wheelbase is denoted as l, and force/torque coefficient of motor is denoted as K_T and K_M, and z_t denotes the distance from the force plane to O_b. Besides, $e_x \in \Re^{4\times1}$ denotes the unit directional row vector for x direction, so as the other states, where e_z, e_ϕ, e_θ, and e_ψ are linearly independent. Moreover, Δ_x denotes the parameter in the x-direction of the uncertain matrix $\Delta \boldsymbol{B}$, Δ_y in the y-direction, and so forth, which are all unknown.

Then the equation of motion can be reorganized as

$$\ddot{\boldsymbol{\eta}} = \dot{\boldsymbol{J}}\boldsymbol{\nu} + \boldsymbol{J}\dot{\boldsymbol{\nu}} = \boldsymbol{B}_e(\beta)\boldsymbol{u} + \boldsymbol{f}(\boldsymbol{\eta}, \dot{\boldsymbol{\eta}}) \qquad (7)$$

where

$$\boldsymbol{B}_e(\beta) = \boldsymbol{J}\boldsymbol{M}^{-1}\boldsymbol{B}(\beta) \qquad (8)$$
$$\boldsymbol{f}(\boldsymbol{\eta}, \dot{\boldsymbol{\eta}}) = (\dot{\boldsymbol{J}} - \boldsymbol{J}\boldsymbol{M}^{-1}\boldsymbol{C} - \boldsymbol{J}\boldsymbol{M}^{-1}\boldsymbol{D})\boldsymbol{J}^{-1}\dot{\boldsymbol{\eta}} - \boldsymbol{J}\boldsymbol{M}^{-1}\boldsymbol{g}(\boldsymbol{\eta}). \qquad (9)$$

Due to its symmetrical features, Mirs-Alioth can be decoupled into several subsystems for easier analysis, as commonly done in complex nonlinear systems as illustrated in [34]. Then the subsystem model can be shown as

$$\ddot{\boldsymbol{\eta}}_i = \boldsymbol{B}_{ei}(\beta)\boldsymbol{u}_i + \boldsymbol{f}(\boldsymbol{\eta}_i, \dot{\boldsymbol{\eta}}_i) \quad (i = 1, \ldots, 4). \qquad (10)$$

Different subsystems, each with specific input constraints, are represented based on the selected index i, where $i = 1$ corresponds to the longitudinal subsystem, and so on. Specifically, the longitudinal subsystem has states $\eta_1 = [x \ z \ \theta]^T$. The transverse subsystem has states $\eta_2 = [y \ z \ \phi]^T$. The heading subsystem is represented by the yaw angle $\eta_3 = \psi$, and the heave subsystem is defined solely by the vertical position $\eta_4 = z$.

III. SINGULAR THRUST TILT ANGLE

In this section, STTA is defined and derived from the model established and then used to demonstrate and prove its capability for generating underwater leveling motion. Then three crucial problems are further raised in the analysis part.

A. Definition and Derivation

The specific thrust tilt angle leading to the singularity is defined as STTA. Intuitively, under STTA, there is no torque generated by thrust on the body, except torque around z-axis. Therefore, except for yaw, the thrust only leads to linear motion without affecting the angular motion of the fuselage. Underwater leveling motion is described as maintaining a level attitude while moving underwater. Therefore, motions based on STTA align with the description of underwater leveling motion, positioning STTA as a significant tool in this study. These motions include longitudinal/lateral slip (turning) motion. Mathematically, a clear definition of a collection of all STTAs of Mirs-Alioth as $\boldsymbol{T}$ is given, containing four elements derived from subsystem (10), combining with the definitions from (3) to (9)

$$\boldsymbol{T} = \{\beta_\phi^*, \ \beta_\theta^*, \ \beta_\psi^*, \ \beta_{heave}^*\} \qquad (11)$$

where

$$\begin{cases} \beta_\phi^* = \arcsin\left(\frac{f(\Delta_y, \Delta_\phi)}{\sqrt{a_\phi^2 + b_\phi^2}}\right) - \arctan\left(\frac{b_\phi}{a_\phi}\right), & (12a) \\[2ex] \beta_\theta^* = \arcsin\left(\frac{f(\Delta_x, \Delta_\theta)}{\sqrt{a_\theta^2 + b_\theta^2}}\right) - \arctan\left(\frac{b_\theta}{a_\theta}\right), & (12b) \\[2ex] \beta_\psi^* = \arcsin\left(\frac{\Delta_\psi}{\sqrt{a_\psi^2 + b_\psi^2}}\right) - \arctan\left(\frac{b_\psi}{a_\psi}\right), & (12c) \\[2ex] \beta_{heave}^* = \arcsin\left(\frac{\Delta_z}{K_T}\right) & (12d) \end{cases}$$

with $a_\phi = -lK_T M_{22}$, $b_\phi = M_{14}K_T - K_M M_{22} + z_t K_T M_{22}$, $a_\theta = lK_T M_{11}$, $b_\theta = M_{15}K_T - K_M M_{11} - z_t K_T M_{11}$, $a_\psi = K_M$, $b_\psi = -K_T l$, $f(\Delta_y, \Delta_\phi)$ is the function of unknown disturbance in the y-direction and ϕ-direction, and so fourth.

Proof: Detailed proofs are found in the supplemental appendix file. □

B. Motions Analysis

In continuation of the previous definition and derivation, numerous points for discussion are conducted for the underwater leveling motion generation utilizing STTA as follows.

1) Operating on STTA: Specifically, observing (12), it is clear that STTA is related not only to internal properties but also to model uncertainties and external disturbances. This implies that STTA is not a time-invariant value, making the values obtained through measurement and modeling in the thrust tilt angle control loop unreliable as desired values. Given the descriptions of underwater leveling motion, the attitude angle can be used as the state variable in the thrust tilt angle control loop. This allows for real-time control of the thrust tilt angle to ensure the vehicle can achieve underwater leveling motion, as detailed in the STTA controller in Section IV. Additionally, referring to the CEM (3), it is evident that for longitudinal slip motion, the thrust tilt angle needs to operate on the STTA of pitch (β_θ^*). Similarly, for lateral slip motion, the thrust tilt angle should work on the STTA of roll (β_ϕ^*). Moreover, it is evident that $\beta_\theta^* \neq \beta_\phi^*$ implies that the control input β is not possible for both the roll and pitch channels to simultaneously operate at STTA, which is the motivation of a switch design illustrated in the next section.

2) Coupling Effects/Control Directional Uncertainty: Generally, as illustrated in Section III, if the vehicle is positioned at STTA, it can generate underwater leveling motions. According to the description of subsystem, combined with two other independent subsystems, a series of composite motions can be produced. For instance, by integrating the heading subsystem, underwater leveling turning motion can be realized. However, as indicated by (7), (8), and (9), the generation of pitch and yaw angles will cumulatively produce a roll angle. Although the vehicle is controlled to a no-pitch condition, there will inevitably be some control errors and fluctuations. Therefore, when generating its turning motion, additional attitude angles will be induced, causing the vehicle to deviate. Thus, it is necessary to consider incorporating an auxiliary controller to ensure that the vehicle maintains a stable attitude angle even when generating composite motions. However, when composite motions are generated, other issues arise. Taking lateral slip turning motion as an example when the thrust tilt angle is β_ϕ^*, a pitch angle is superimposed, making the CEM of this channel partially unknown according to (7). Hence, using the controller to stabilize the pitch at this point can be considered a problem of control directional uncertainty, which is the primary motivation for using the Nussbaum function in Section IV.

IV. UNDERWATER LEVELING MOTION SCHEME

In this section, a detailed description of Aqua Slide is given. The whole aquatic control strategy is outlined in Fig. 3, with the Aqua Slide marked in blue color. Firstly, a mode-switching term, utilizing δ_{RC} (inputs from the remote controller) and z_r (desired depth), facilitates transitions between operational modes. It is designed as a logic algorithm to switch between different modes depending on signals from the remote controller. Specifically, the mode switch algorithm operates as follows. If
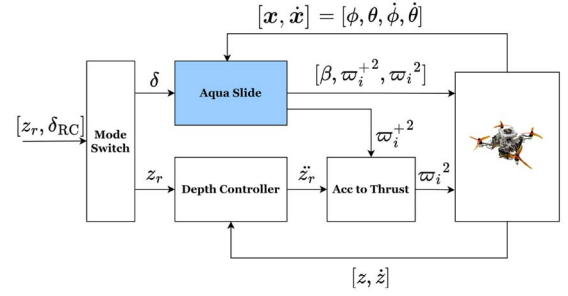

Fig. 3. Overview of the aquatic control strategy diagram. Aqua Slide is marked in blue color.
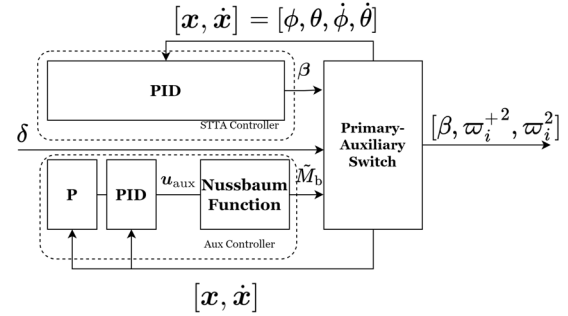

Fig. 4. Detailed scheme diagram of Aqua Slide.

z_r is invalid, switch δ to δ_{RC}, deactivate the depth controller, and activate alternative modes [16] or Aqua Slide. Otherwise, reset δ to 0 and activate the depth controller. Except for the STTA mode, which is controlled by the Aqua Slide, and depth mode, some other modes are all open-loop. And the details are found in [16]. Next, a depth control strategy using a cascaded P-PID control scheme maintains operational depth. Additionally, a computational block converts acceleration to body-frame thrust [35].

The novel scheme, named Aqua Slide, detailed in Fig. 4, is developed based on the analysis in Sections III-A and III-B. It regulates the vehicle using the STTA/singularity, taking $\boldsymbol{\delta} = [\delta_x \ \delta_y]^T$ as the desired throttle components and outputting ϖ_i^+ as motor speed via an auxiliary controller.

As per the description of underwater leveling motion in Section III, the desired attitudes are all determined as zero. As presented in Fig. 4 and the analysis in Section III-B1, a PID controller is specifically deployed for attitude regulation within the STTA framework by

$$\boldsymbol{\beta} = -\text{sgn}(\boldsymbol{\delta}) \left(\mathbf{K}_{\mathbf{P}\beta} \boldsymbol{x} + \mathbf{K}_{\mathbf{D}\beta} \dot{\boldsymbol{x}} + \mathbf{K}_{\mathbf{I}\beta} \int \boldsymbol{x} \mathrm{d}t \right) \quad (13)$$

where $\boldsymbol{\beta} = [\beta_\theta, \beta_\phi]$, $\mathbf{K}_{\mathbf{P}\beta}$, $\mathbf{K}_{\mathbf{D}\beta}$, and $\mathbf{K}_{\mathbf{I}\beta}$ are the positive proportional, derivative, and integral gains for controller, respectively. $\text{sgn}(\cdot)$ is a sign function.

As the analysis in Section III-B1, a primary channel and an auxiliary channel are introduced. An algorithm is proposed for switching between each other depending on specific operational scenarios. As outlined in the Algorithm 1, to preclude the simultaneous execution of roll and pitch motions.

Algorithm 1 Primary-Auxiliary Switch

1: **Input:** $\delta_{\mathrm{x}}, \delta_{\mathrm{y}}$
2: **Output:** $\beta, {\varpi_i}^2, {\varpi_i^+}^2$
3: **if** $|\delta_{\mathrm{x}}| \geq |\delta_{\mathrm{y}}|$ **then**
4: $\quad \beta = \beta_\theta^*$ //Pitch is primary channel;
5: $\qquad$ //Roll is auxiliary channel;
6: **else**
7: $\quad \beta = \beta_\phi^*$ //Roll is primary channel;
8: $\quad \dagger = \theta$ //Pitch is auxiliary channel;
9: **end if**
10: ${\varpi_i^+}^2 = \mathcal{H} \cdot (\mathrm{Normalize}(\tilde{\boldsymbol{M}}_{\mathrm{b}}));$
11: ${\varpi_i}^2 = \mathcal{H} \cdot \boldsymbol{\delta} + {\varpi_i^+}^2;$

This state machine serves a dual function: it not only ensures the mutual exclusivity of roll and pitch motions but also facilitates the dynamic interchange between the primary and auxiliary control channels, and passes the values to the mixer module in PX4 flight stack eventually [35]. The defined $\mathcal{H} \in \Re^{4\times 2}$ is a modified mixer matrix, constructed by selecting the roll and pitch channels from the standard mixer matrix.

In addition, as the analysis in Section III-B2, an auxiliary controller is designed to ensure the stability of the auxiliary channel while the primary channel is regulated by the controller in (13). This is further complicated by the uncertainty in the control direction, which is due to the variable nature of $\boldsymbol{B}_{\mathrm{e}}$, as outlined in (7). A saturated Nussbaum gain function is employed as

$$\tilde{\boldsymbol{M}}_{\mathrm{b}} = \boldsymbol{\mathcal{N}}(\zeta_\phi, \zeta_\theta)\boldsymbol{u}_{\mathrm{aux}} \tag{14}$$

$$\boldsymbol{\mathcal{N}}(\zeta_\phi, \zeta_\theta) = \mathrm{diag}[\mathcal{N}(\zeta_\phi), \mathcal{N}(\zeta_\theta)] \tag{15}$$

$$\mathcal{N}(\zeta_\dagger) = \mathrm{Sat}(\bar{\mathcal{N}}(\zeta_\dagger)) \tag{16}$$

$$\bar{\mathcal{N}}(\zeta_\dagger) = \cos\frac{\pi \cdot \zeta_\dagger}{2} \cdot e^{\zeta_\dagger^2} \tag{17}$$

$$\dot{\zeta}_\dagger = \mathrm{K}_{\zeta,\dagger} \cdot |^{\mathrm{b}}\boldsymbol{\omega}_\dagger| \cdot |\boldsymbol{u}_{\mathrm{aux},\dagger}| \tag{18}$$

where $\dagger \in [\phi, \theta]$ stands for the specific element index in a vector. The current angular velocity is denoted as $^{\mathrm{b}}\boldsymbol{\omega}_\dagger$. The standard Nussbaum function is defined as $\bar{\mathcal{N}}(\zeta_\dagger)$, with ζ as the state of this function, modulated by a gain $\mathrm{K}_{\zeta,\dagger}$ for the channel of $\dagger$. Notice $\boldsymbol{u}_{\mathrm{aux},\dagger}$ is an element of input $\boldsymbol{u}_{\mathrm{aux}}$ of a channel of $\dagger$, and $\mathrm{Sat}(\cdot)$ is a saturated function.

Moreover, the $\boldsymbol{u}_{\mathrm{aux}}$ is the output of a cascade P-PID controller, which can be expanded as

$$\dot{\boldsymbol{x}}_{\mathrm{d}} = -\mathbf{K}_{\mathbf{P}\boldsymbol{x}}\boldsymbol{x} \tag{19}$$

$$\boldsymbol{u}_{\mathrm{aux}} = \mathbf{K}_{\mathrm{p}}(\dot{\boldsymbol{x}}_{\mathrm{d}} - \dot{\boldsymbol{x}}) + \mathbf{K}_{\mathrm{d}}(\ddot{\boldsymbol{x}}_{\mathrm{d}} - \ddot{\boldsymbol{x}}) + \mathbf{K}_{\mathrm{i}}\int(\dot{\boldsymbol{x}}_{\mathrm{d}} - \dot{\boldsymbol{x}})\mathrm{d}t \tag{20}$$

where $\dot{\boldsymbol{x}}_{\mathrm{d}}$ is the output of the P controller and also the desired value of the PID controller, $\mathbf{K}_{\mathbf{P}\boldsymbol{x}}$ is the proportional gain matrix for attitude auxiliary controller, $\mathbf{K}_{\mathrm{p}}$, $\mathbf{K}_{\mathrm{d}}$, and $\mathbf{K}_{\mathrm{i}}$ are the proportional, derivative, and integral gains matrix for attitude rate auxiliary controller, respectively.

A. Nussbaum Function

From [28], a function can be treated as a Nussbaum function if it has the property shown as follows:

$$\lim_{s\to\infty}\sup\int_{s_0}^s \bar{\mathcal{N}}(\zeta_\dagger) = +\infty, \lim_{s\to\infty}\inf\int_{s_0}^s \bar{\mathcal{N}}(\zeta_\dagger) = -\infty.$$

Throughout this article, an even standard Nussbaum function is considered in (17).

Remark 1: From the property that a standard Nussbaum function has shown above, it is obvious that the saturated Nussbaum function (16) is bounded.

B. Stability Analysis

Due to the characteristics of Algorithm 1 and the previously described model, the stability proof of the entire attitude loop can be divided into two parts. One part addresses the stability of the primary channel, while the other deals with the stability of the auxiliary channel. We consider the case where ϕ is the primary channel and θ is the auxiliary channel. An assumption is given based on the requirement that the leveling motion is to be generated by the vehicle.

Assumption 1: The Euler angles are treated as minor values. Therefore, $s_\phi \approx \phi$, $c_\phi \approx 1$, the same for θ.

Assumption 2: The lump uncertain matrix in (3) is continuously differentiable, and they and their time derivatives are bounded, in such that $\sup_{t\geq 0}|\Delta_\phi| < \infty$, $\sup_{t\geq 0}|\Delta_\theta| < \bar{\Delta} < \infty$, $\bar{\Delta}$ is an unknown constant.

1) Primarily Channel: Under the Assumption 1, based on (1)–(2), (3), (14) and Algorithm 1, the model of the main channel can be described as a nonaffine uncertain nonlinear model

$$\dot{\phi} = p \tag{21}$$

$$\dot{p} = f_{\mathrm{p}}(\phi, p, \beta_\phi, \Delta_\phi) \tag{22}$$

with

$$f_{\mathrm{p}}(\phi, p, \beta_\phi, \Delta_\phi) = \frac{1}{M_{44}}(-(I_{\mathrm{rr}}r - N_{\dot{r}}r)q - K_{\mathrm{p}}p - \Delta z B\phi + (k_1(\beta_\phi) + \sqrt{2}\Delta_\phi)\delta_{\mathrm{y}}. \tag{23}$$

where Δz is the distance between CoG and CoB.

Then we define a function space,

$$\mathcal{F} = \left\{ \left|\frac{\partial f_{\mathrm{p}}}{\partial \phi}\right| \leq \Delta z B, \left|\frac{\partial f_{\mathrm{p}}}{\partial p}\right| \leq K_{\mathrm{p}}, \frac{\partial f_{\mathrm{p}}}{\partial \beta_\phi} \geq \underline{b}, \right.$$
$$\left. \left|\frac{\partial f_{\mathrm{p}}}{\partial \beta_\phi}\right| \leq \bar{b}, \forall \phi, p, \beta_\phi \right\} \tag{24}$$

where $0 < \underline{b} \leq \bar{b}$ are constants. We neglect the stochastic terms present in the original work [36]. Therefore, the key parameters N_1 and N_2, are treated as arbitrary positive constants.

A parameter set is further defined

$$\Omega = \left\{ k_{\mathrm{p}\beta\phi}^2 > 2k_{\mathrm{i}\beta\phi}k_{\mathrm{d}\beta\phi} + \bar{k} + N_1^2 k_{\mathrm{d}\beta\phi}/\underline{b} \right.$$
$$\left. k_{\mathrm{d}\beta\phi}^2 > k_{\mathrm{p}\beta\phi}/\underline{b} + \bar{k} + N_2^2 k_{\mathrm{d}\beta\phi}/\underline{b} \right\} \tag{25}$$

where $\bar{k} \triangleq (\Delta z B + K_{\mathrm{p}})(k_{\mathrm{p}\beta\phi} + k_{\mathrm{d}\beta\phi})/\underline{b}$.

Theorem 1: ([36], Them. 3.6) Consider a system (21)–(22). Under the Assumption 2, then for any PID control parameters $(k_p, k_i, k_d) \in \Omega$, such that the nonlinear uncertain function $f \in \mathcal{F}$, any constant setpoint ϕ_d, any initial state ϕ_0, p_0, the closed-loop system is globally stable and regulated.

Remark 2: From Theorem 1, we can easily deduce that when the PID parameters satisfy the required conditions stated above, the controller (13) ensures the global stability of our system (21)–(22).

2) Auxiliary Channel: Next, we discuss the stability of the auxiliary channel. We first give the following lemma.

Lemma 1: [37] Let $V(\cdot)$ and $\zeta(\cdot)$ be smooth functions defined on $[0, t_f]$ with $V(t) \geq 0, \forall t \in [0, t_f]$, $\bar{\mathcal{N}}(\cdot)$ be an even smooth Nussbaum-type function, $c_0 > 0$ and $c_1 > 0$ are suitable constants, $\alpha(\tau)$ be time-varying parameter which takes values in the unknown closed intervals $L = [l^-, l^+]$, with $0 \notin L$. If the following inequality holds:

$$V(t) < c_0 + e^{-c_1 t} \int_0^t \left(\alpha(\tau)\bar{\mathcal{N}}(\zeta(\tau)) + 1 \right) \dot{\zeta}(\tau) e^{c_1 t} d\tau$$

then $V(t)$, $\zeta(t)$, and $\int_0^t \left(\alpha(\tau)\mathcal{N}(\zeta(\tau)) + 1 \right) \dot{\zeta}(\tau) e^{c_1 t} d\tau$ must be bounded on $[0, t_f]$.

Remark 3: Lemma 1 holds for the standard case of Nussbaum function (17). It is evident that when the Nussbaum function has upper and lower bounds as illustrated in Remark 1, Lemma 1 remains valid.

The auxiliary channel model is described as

$$\dot{\theta} = q \tag{26}$$
$$\dot{q} = f_q(q, \theta) + b\mathcal{N}(\zeta_\theta)u_{\text{aux},\theta} \tag{27}$$

where $b = (k_2 + \sqrt{2}\Delta)/M_{55}$, $f_q(q, \theta) = (-C_5 p - M_q q - \Delta z B \theta)/M_{55}$.

From the controller from (19) to (20), we define the error $e = q_d - q$, and the PID parameters $K_p = 10\gamma K_d$, $K_i = \gamma^2 K_d$. Then the input can be reorganized as

$$u_{\text{aux},\theta} = K_d E \tag{28}$$

where $E \in \mathbb{R}$ and $E = 10\gamma e + \gamma^2 \int e \, d\tau + \dot{e}$, γ is a user-designed positive parameter making $e^2 + 10\gamma e + \gamma^2$ is Hurwitz. It is provable that the boundedness of E ensures the boundedness of each element [38]. Therefore, one can transfer the target from e to make sure E is globally uniformly ultimately bounded (GUUB). Then the derivative of E can be organized as

$$\dot{E} = 10\gamma\dot{e} + \gamma^2 e + \ddot{e}$$
$$= -K_{P\theta}b\mathcal{N}u_{\text{aux},\theta} + 10\gamma\dot{e} + \gamma^2 e - K_{P\theta}f_q - \ddot{q}$$
$$= \mathcal{B}\mathcal{N}u_{\text{aux},\theta} + H(q) \tag{29}$$

Property 1: There exist a nonnegative constant a_f and a nonnegative scalar function φ_f, such that $|f_q(q, \theta)| \leq a_f \varphi_f$.

Therefore, according to Property 1, (29) is upper bounded as

$$|H(q)| \leq a\varphi(\cdot) \tag{30}$$

where a is an undetermined constant and $\varphi(\cdot)$ is a computable scale function, with $a = \max\{K_{P\theta}a_f, \ 10\gamma, \ \gamma^2\}$ and $\varphi(\cdot) = \varphi_f + |\dot{e}| + |e|$.

Theorem 2: Consider a system that described by (26)–(27). If the controllers (19)–(20) have parameter settings that locate in a parameter set

$$\Omega_q = \{1 \leq K_{\zeta\theta}, \ a\varphi^2(\cdot) \leq K_{\zeta\theta}K_d,$$
$$0 < \gamma \leq K_{P\theta} + 1\} \tag{31}$$

and the system possesses Property 1, GUUB tracking error of the system can be ensured.

Proof: Consider the following Lyapunov function candidates:

$$V_1 = \frac{1}{2}E^2. \tag{32}$$

With (28), (29), and (30), the time derivative of V_1 is

$$\dot{V}_1 = E\dot{E} = EH(q) + \mathcal{B}K_d\mathcal{N}(\zeta_\theta)|E|^2$$
$$\leq a\varphi(\cdot)|E| + \mathcal{B}K_d\mathcal{N}(\zeta_\theta)|E|^2$$
$$\leq a\varphi^2(\cdot)|E|^2 + \frac{a}{4} + \mathcal{B}K_d\mathcal{N}(\zeta_\theta)|E|^2. \tag{33}$$

With tuning the PID parameters into the parameter set (31), then the inequality holds

$$\dot{V}_1 \leq K_{\zeta\theta}K_d|E||q| + \mathcal{B}K_dK_\zeta\mathcal{N}(\zeta_\theta)|E||q| + \frac{a}{4}$$
$$\leq (\mathcal{B}\mathcal{N}(\zeta_\theta) + 1)\dot{\zeta} + \frac{a}{4}. \tag{34}$$

Let $c_1 > 0$ being a constant and multiply (34) by $e^{c_1 t}$ and integrate both sides of it in $[0, t_f]$ yields

$$V_1(t) \leq \frac{a}{4c_1} + V_1(0) + e^{-c_1 t}\int_0^t (\mathcal{B}\mathcal{N}(\zeta_\theta) + 1)\dot{\zeta}e^{c_1 t}d\tau. \tag{35}$$

Since $V_1(0)$ and $\int_0^t \left(\alpha(\tau)\mathcal{N}(\zeta) + 1\right)\dot{\zeta}e^{c_1 t}d\tau$ are bounded, then from (32) and (35), it can be concluded that

$$\lim_{t \to \infty} \frac{1}{2}|E|^2 \leq \frac{a}{4c_1} \tag{36}$$

implying that $|E|$ converges into a residual set $\{|E| \mid |E| \leq \sqrt{(a/2c_1)}\}$ ultimately. Similarly, e ultimately converges to a small residual set. Clearly, for the strict-feedback system (26)–(27), given that $\theta_d = 0$, under the time scale separation assumption and $K_{P\theta} \in \Omega_q$, θ converges to a small residual set. □

V. VALIDATION: SIMULATIONS AND EXPERIMENTS

Based on the proposed control framework, the simulations and experiments are introduced in this section. A brief introduction to the Gazebo-HITL setup is given. Then simulations of the entire cycle and two comparative tests were conducted on a self-established simulation platform, followed by physical experiments replicating these tests.

A. Gazebo-HITL Simulation

Even though existing various simulations for both aerial or underwater robotics [39], [40], their works are based on Matlab or without considering the real onboard computational units. To narrow the gap between the simulation and the physical prototype, we built a simulation environment using a HITL setup with Gazebo 11.3 and Pixhawk 4 Mini, and the comparative
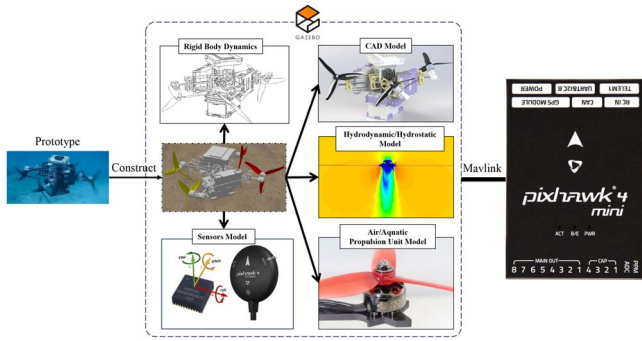
Fig. 5. Setup of the Gazebo-HITL simulation.

figures between the prototype and the simulation are found in Fig. 2. Concretely, the setup of the simulation architecture is shown in Fig. 5.

First, the identified parameters of the mathematical model used in the Gazebo simulation [33]. Secondly, the proposed controllers run on the Pixhawk flight controller but interact with the simulation through serial interfaces. The simulation covers as much as possible components in the prototype, including the effects of the hydrodynamics and the coupling. Except that, the noise and the computational capabilities of the flight controller are also considered. In addition, under the premise of satisfying the PID function space (25) and (31) discussed in the stability analysis, we designed the PID parameters for the simulation and made slight adjustments based on the response results Table I.

Fig. 6 illustrates the trajectory of the simulation and Fig. 7 presents a detailed response of each state. Specifically, as shown in the yellow section of Fig. 7, the roll channel is the primary channel for generating lateral slip turning motion. This is in line with Algorithm 1, where $\beta = \beta_\phi^*$ at this point. At 25 s, the auxiliary controller within the control framework stabilizes the pitch angle generated by the compounded yaw angle. Although the Nussbaum function introduced approximately 5.7° of overshoot in compensating for the issue of control direction uncertainty, it ultimately stabilizes the entire system. In terms of the response of the roll channel, the approximately 12° of overshoot originate from the switching process between different modes.

Under the same conditions, the control situation of roll and pitch angles without introducing the Nussbaum function in the auxiliary controller can be observed from Fig. 9. This comparative simulation disables the Nussbaum function at point "a" and leads to pitch angle non-convergence until it re-enables at point "b". Since the roll angle is not the control target of the auxiliary controller, its influence is minimal throughout the process. Additionally, the curve in the blue and purple area indicates that focusing on STTA of the pitch with the STTA controller also stabilizes roll via the auxiliary controller. Additionally, as shown in Fig. 8, the CPU loading throughout the simulation cycle remains relatively low, ranging from a minimum mean value of 57.33% to a maximum mean value of 58.33%. There are slight fluctuations in CPU loading under different modes. The blue and yellow modes require more computational resources

than the green and gray modes. In general, the more modules of Aqua Slide that are invoked, the more CPU resources are consumed. Two comparative simulations in Fig. 10 shows that without this auxiliary controller, the secondary channel grows with the turning radius and fails to converge to zero.

B. Physical Experiments

Guided by the parameters setting in the Gazebo-HITL simulation stated in the last section, a series of parameters for controllers are determined as shown in Table I. As illustrated in Fig. 11, the physical experiment encompassed a complete cycle of lateral slip turning mode followed by longitudinal slip (turning) mode. The flight controller shown in Fig. 5 is transplanted in the prototype to finish the physical experiments. From Fig. 11(b), both the roll and pitch angles undergo minimal changes throughout the cycle, with the peak values of both angles not exceeding 5°. Before 10 s, the vehicle performs a lateral slip turning mode, transitioning to longitudinal slip (turning) mode thereafter.

Throughout the process, Aqua Slide demonstrated real-time performance despite perturbations from by the long mechanical transmission chain or process during switching. As shown in Fig. 11(b), during mode switching at 10 s, the thrust tilt angle shifted from β_ϕ^* to β_θ^*, and within 2 s, Aqua Slide stabilized the attitude angle. After 12 s, multiple longitudinal slip turning motions were performed, and the control system quickly suppressed the coupling effects. For example, between 30 and 32.5 s, the vehicle experienced wall effects causing roll oscillations within [−4.9°, 3.44°], but these were stabilized within 1.5 s. Although minor fluctuations in pitch and roll still existed after stabilization, they were generally negligible. The experiments in Fig. 11 were conducted in a confined environment, where boundary effects influence Mirs-Alioth's operation. It demonstrates resistance to boundary-induced disturbances, confirming the effectiveness of our proposed scheme in confined spaces.

Furthermore, the outputs of the Nussbaum function, are depicted in Fig. 11(b), indicating that it effectively compensates for the problem of control direction uncertainty. One notices that the pitch channel exhibits both positive and negative adjustments, whereas the roll channel does not. This indicates that when the roll channel serves as the primary channel, the auxiliary channel (pitch) experiences control direction uncertainty. Conversely, when the pitch channel is primary and roll is auxiliary, no control direction uncertainty occurs. In this case, the Nussbaum function primarily compensates for uncertainties or nonlinearity.

Fig. 13 reveals the CPU usage of the flight control board during the experiment when running Aqua Slide. It shows that while the CPU loading fluctuates over time, the average remains relatively low at 58.49%. Comparing this with the CPU loading in the simulation, as shown in Fig. 8, the CPU usage in both scenarios is very similar. This suggests that the gap between the computational capabilities of the simulation environment and the real robot is minimal. Consequently, it is feasible to directly transfer the algorithm from the HITL simulation to the physical robot.

TABLE I
PARAMETERS OF CONTROLLERS FOR SIMULATION AND EXPERIMENT

|	$\mathbf{K_{P\beta}}$	$\mathbf{K_{I\beta}}$	$\mathbf{K_{D\beta}}$	$\mathbf{K_{Px}}$	$\mathbf{K_p}$	$\mathbf{K_i}$	$\mathbf{K_d}$	$\mathbf{K_\zeta}$
Simulation	$\begin{bmatrix} 5 & 0 \\ 0 & 5 \end{bmatrix}$	$\begin{bmatrix} 0.9 & 0 \\ 0 & 0.9 \end{bmatrix}$	$\begin{bmatrix} 0.5 & 0 \\ 0 & 0.5 \end{bmatrix}$	$\begin{bmatrix} 5 & 0 \\ 0 & 10 \end{bmatrix}$	$\begin{bmatrix} 0.1 & 0 \\ 0 & 0.1 \end{bmatrix}$	$\begin{bmatrix} 0.01 & 0 \\ 0 & 0.01 \end{bmatrix}$	$\begin{bmatrix} 0.01 & 0 \\ 0 & 0.01 \end{bmatrix}$	$\begin{bmatrix} 4.5 & 0 \\ 0 & 4.5 \end{bmatrix}$
Experiment	$\begin{bmatrix} 2 & 0 \\ 0 & 1.5 \end{bmatrix}$	$\begin{bmatrix} 0.5 & 0 \\ 0 & 0.5 \end{bmatrix}$	$\begin{bmatrix} 0.1 & 0 \\ 0 & 0.1 \end{bmatrix}$	$\begin{bmatrix} 5 & 0 \\ 0 & 10 \end{bmatrix}$	$\begin{bmatrix} 0.3 & 0 \\ 0 & 0.9 \end{bmatrix}$	$\begin{bmatrix} 0.01 & 0 \\ 0 & 0.01 \end{bmatrix}$	$\begin{bmatrix} 0.01 & 0 \\ 0 & 0.01 \end{bmatrix}$	$\begin{bmatrix} 4.3 & 0 \\ 0 & 4.3 \end{bmatrix}$
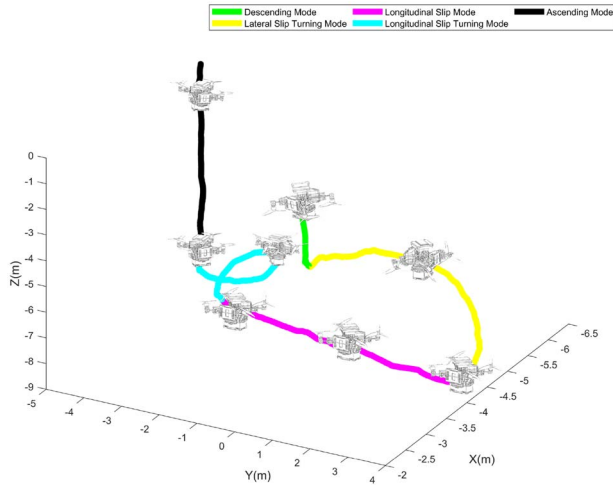
Fig. 6. Trajectory plots of the whole simulation cycle. Proceeded by MATLAB of the Gazebo-HITL simulation in 3-D, side, and top view. The vehicle begins with a vertical descent along the green line, performs a lateral slip (turning) motion on the yellow line, spirals down, continues with a longitudinal slip on the magenta line, spirals upward during a longitudinal turning motion on the cyan line, and concludes with a vertical ascent on the black line.
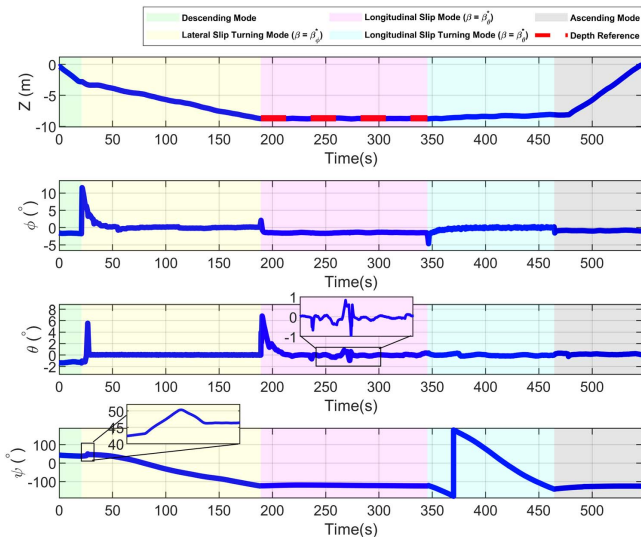

Fig. 7. Results of the whole simulation cycle. The colorful backgrounds stand for various operating modes.

Besides, two comparative physical experiments are conducted, one without the Nussbaum function and another without an auxiliary controller as shown in Fig. 12. As shown in
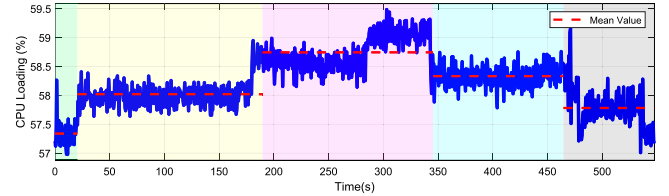

Fig. 8. CPU Loading in the simulation cycle. Sharing the same legends as the Fig. 7.
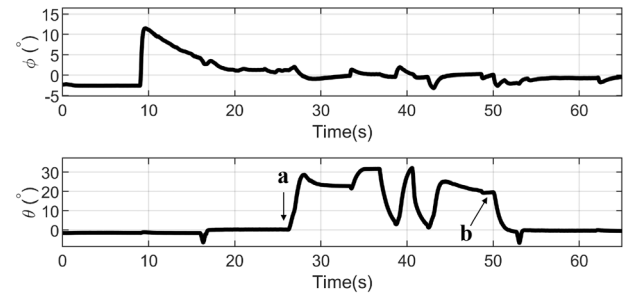

Fig. 9. Comparison simulation of with and without Nussbaum function. The Nussbaum function is disabled at the point **a** and re-enabled at the point **b**.
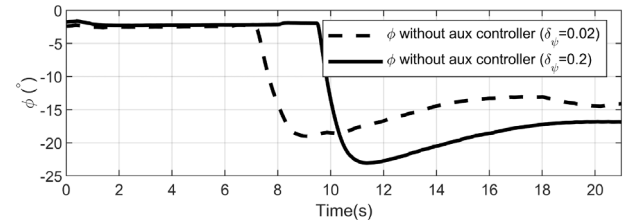

Fig. 10. Comparison simulation of without auxiliary controller under different yaw inputs.

Fig. 12(a), when the vehicle is required to conduct lateral turning motion, it faces severe instability without the incorporation of the Nussbaum function, rendering the attitude uncontrollable. Moreover, the attitude results in Fig. 12(b) imply that the roll and pitch angle of the vehicle increase dramatically. The other comparative physical experiment, presented in Fig. 12(c) and Fig. 12(d), demonstrates the importance of the auxiliary controller. As observed in Fig. 12(c), even though the vehicle does not experience the severe instability seen in the physical experiment without the Nussbaum function, it still exhibits significant attitude change during turns. It corroborates the analysis presented earlier and indirectly confirms the validity of
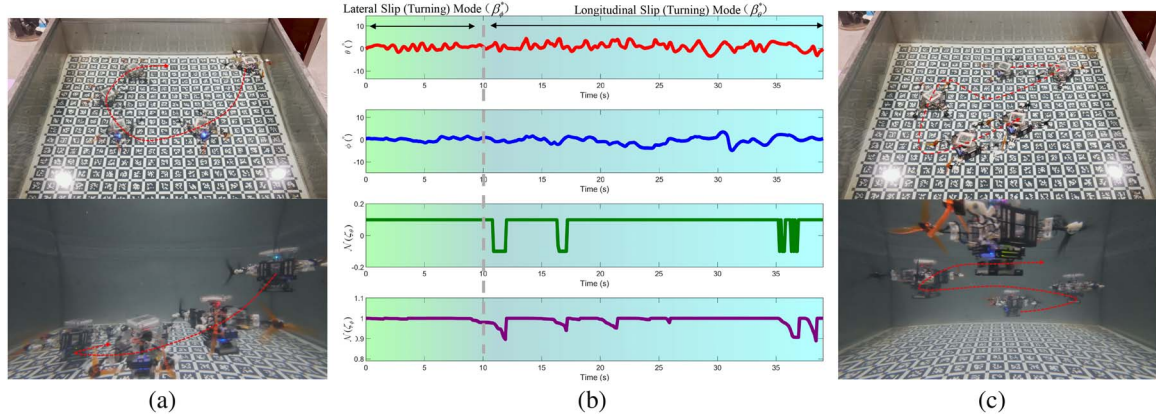
Fig. 11. Physical experiment of both lateral slip (turning) motion and longitudinal slip (turning) motion. (a) Snapshots of lateral slip (turning) motion. (b) Results of the complete lateral slip (turning) motion and longitudinal slip (turning) motion cycle. (c) Snapshots of longitudinal slip (turning) motion. Colorful backgrounds correspond to different modes.
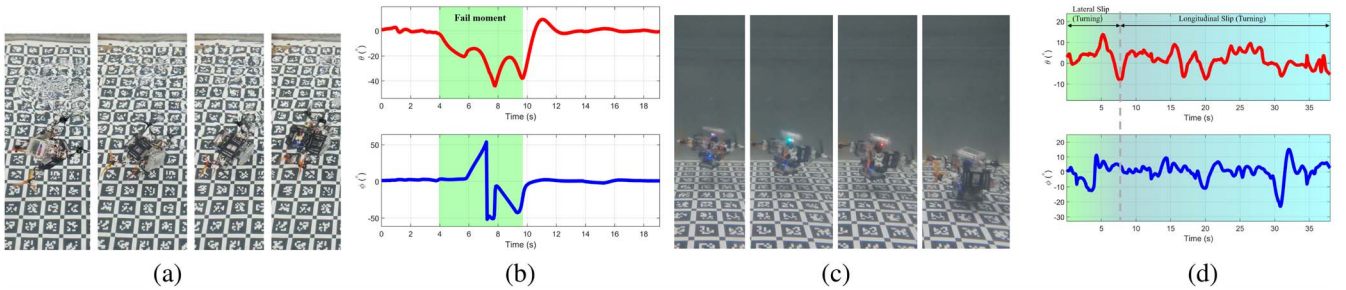
Fig. 12. Comparative physical experiments. (a) Snapshot of the fail moment in the physical experiment without the Nussbaum function. (b) Attitude response during the experiment without Nussbaum function. (c) Snapshot of the moment the vehicle started rolling in the physical experiment without the auxiliary controller. (d) Attitude response during the experiment without the auxiliary controller.
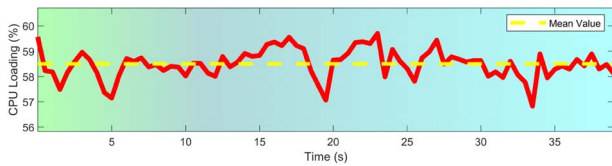
Fig. 13. CPU loading during the experiment.

the motion analysis. Specifically, the attitude results shown in Fig. 12(d) reveal that before 8 s, the vehicle undergoes lateral slip turning motion, followed by longitudinal slip motion. Compared with the attitude angle changes in Fig. 12(b), the peak pitch angle increases to 13°, and the peak roll angle escalates to 23°. As described in Algorithm 1, when the roll is the primary channel, the auxiliary controller operates on the pitch channel. Therefore, during lateral slip turning motion, the pitch channel experiences greater fluctuations due to the lack of assistance from the auxiliary controller, and similarly for longitudinal turning motion.

Additionally, an intriguing phenomenon is emerges: in the simulations, the roll channel is minimally affected by disabling the Nussbaum function, as shown in Fig. 9. However, in the physical experiments, the impact is substantial, revealing that the interplay among the attitude channels is significant. This

phenomenon is also reflected in Fig. 12(d), where during the lateral slip turning mode phase, the roll, being the primary channel, should not be affected by disabling the auxiliary controller. Yet, compared to Fig. 11, the peak value of the roll angle evidently exceeds 10°. Therefore, the comparison between these sets and the simulations highlights the critical role of the Nussbaum function and the auxiliary controller in generating underwater leveling motion in an under-actuated tilting M-UAAV.

VI. CONCLUSION

In this article, a novel scheme, Aqua Slide, for M-UAAV in underwater leveling motion has been proposed that utilizes singularity. The definition of STTA has been derived, theoretically utilized, and analyzed for generating underwater leveling motions. Building on the analysis of the STTA, three key problems have been identified the existence of the STTA difference between roll and pitch, controls directional uncertainty, and coupling effect. On this basis, the outline of the Aqua Slide has been proposed to tackle the key problems. The Aqua Slide has been implemented onboard for both self-developed HITL-Gazebo simulations and experiments of prototype Mirs-Alioth. The vehicle is able to operate in underwater uni-directional

leveling motion of the STTA controller and turn through the auxiliary controller and the saturated Nussbaum function.

Furthermore, the cross-validation between the Gazebo-HITL simulations and experiments has been conducted both in a whole cycle test and two comparative tests with/without the Nussbaum function and auxiliary controller. Simulations and experiments have shown that the framework effectively produces underwater leveling motions, managing three key issues. Attitude angle changes have remained below 5° during these motions. Without the Nussbaum function and auxiliary controller, comparative tests have revealed uncontrolled attitude changes with peaks up to 23°, underscoring the critical role of these controls. Some limitations are obvious like no external disturbance (like waves or wind) has been considered in the simulation. Combined with the test pool experiments, this setting is acceptable here but will be refined and open to the public in the future.

REFERENCES

[1] Y. H. Tan and B. M. Chen, "Survey on the development of aerial–aquatic hybrid vehicles," *Unmanned Syst.*, vol. 9, no. 3, pp. 263–282, 2021.

[2] Z. Zeng, C. Lyu, Y. Bi, Y. Jin, D. Lu, and L. Lian, "Review of hybrid aerial underwater vehicle: Cross-domain mobility and transitions control," *Ocean Eng.*, vol. 248, 2022, Art. no. 110840.

[3] B. Huang, H. Peng, C. Zhang, and C. K. Ahn, "Distributed optimal coordinated control for unmanned surface vehicles with interleaved periodic event-based mechanism," *IEEE Trans. Veh. Technol.*, early access, Jul. 23, 2024.

[4] B. Huang, C. Zhu, Y. Xu, G. Zhu, and Y. Su, "Energy tradeoff-oriented quasi-optimal distributed affine formation maneuver control for electric marine surface vehicles," *IEEE Trans. Transp. Electrific.*, early access, Jun. 17, 2024.

[5] M. M. Maia, D. A. Mercado, and F. J. Diez, "Design and implementation of multirotor aerial-underwater vehicles with experimental results," in *Proc. IEEE/RSJ Int. Conf. Intell. Robots Syst. (IROS)*, 2017, pp. 961–966.

[6] Y. Jin, Y. Bi, C. Lyu, Y. Bai, Z. Zeng, and L. Lian, "Nezha-IV: A hybrid aerial underwater vehicle in real ocean environments," *J. Field Robot.*, 2024.

[7] Y. Bi, Y. Jin, C. Lyu, Z. Zeng, and L. Lian, "Nezha-mini: Design and locomotion of a miniature low-cost hybrid aerial underwater vehicle," *IEEE Robot. Automat. Lett.*, vol. 7, no. 3, pp. 6669–6676, Jul. 2022.

[8] X. Liu et al., "TJ-FlyingFish: Design and implementation of an aerial–aquatic quadrotor with tiltable propulsion units," in *Proc. IEEE Int. Conf. Robot. Automat. (ICRA)*, 2023, pp. 7324–7330.

[9] Y. Bai, Y. Jin, C. Liu, Z. Zeng, and L. Lian, "Nezha-F: Design and analysis of a foldable and self-deployable HAUV," *IEEE Robot. Automat. Lett.*, vol. 8, no. 4, pp. 2309–2316, Apr. 2023.

[10] L. Li et al., "An aerial–aquatic hitchhiking robot with remora-inspired tactile sensors and thrust vectoring units," *Adv. Intell. Syst.*, 2023, Art. no. 2300381.

[11] H. Rao et al., "Puffin platform: A morphable unmanned aerial/underwater vehicle with eight propellers," *IEEE Trans. Ind. Electron.*, vol. 71, no. 7, pp. 7621–7630, Jul. 2024.

[12] D. Huang, X. Liu, M. Dou, and B. M. Chen, "Systematizing rotor-based morphable unmanned aerial–aquatic vehicles design: From theory to prototype," in *Proc. OCEANS-Singapore*, 2024, pp. 1–9.

[13] Y. H. Tan and B. M. Chen, "Design of a morphable multirotor aerial–aquatic vehicle," in *Proc. OCEANS MTS/IEEE SEATTLE*, 2019, pp. 1–8.

[14] Y. H. Tan and B. M. Chen, "Underwater stability of a morphable aerial–aquatic quadrotor with variable thruster angles," in *Proc. IEEE Int. Conf. Robot. Automat. (ICRA)*, 2021, pp. 314–320.

[15] A. Dawoud, M. Alam, A. Bal, and C. Loo, "Target tracking in infrared imagery using weighted composite reference function-based decision fusion," *IEEE Trans. Image Process.*, vol. 15, no. 2, pp. 404–410, Feb. 2006.

[16] Y. H. Tan and B. M. Chen, "Thruster allocation and mapping of aerial and aquatic modes for a morphable multimodal quadrotor," *IEEE/ASME Trans. Mechatron.*, vol. 25, no. 4, pp. 2065–2074, Aug. 2020.

[17] L. Sciavicco and B. Siciliano, *Modelling and Control of Robot Manipulators*. Springer-Verlag, 2012.

[18] S. Jin, J. Kim, J. Kim, and T. Seo, "Six-degree-of-freedom hovering control of an underwater robotic platform with four tilting thrusters via selective switching control," *IEEE/ASME Trans. Mechatron.*, vol. 20, no. 5, pp. 2370–2378, Oct. 2015.

[19] Z. Lv, Y. Wu, Q. Zhao, and X. Sun, "Design and control of a novel coaxial tilt-rotor UAV," *IEEE Trans. Ind. Electron.*, vol. 69, no. 4, pp. 3810–3821, Apr. 2022.

[20] T. Xie, B. Xian, X. Gu, J. Hu, and M. Liu, "Disturbance observer-based fixed-time tracking control for a tilt trirotor unmanned aerial vehicle," *IEEE Trans. Ind. Electron.*, vol. 71, no. 4, pp. 3894–3903, Apr. 2024.

[21] K. Bodie, Z. Taylor, M. Kamel, and R. Siegwart, "Towards efficient full pose omnidirectionality with overactuated MAVs," in *Proc. Int. Symp. Exp. Robot.*, Springer-Verlag, 2020, pp. 85–95.

[22] M. Allenspach et al., "Design and optimal control of a tiltrotor micro-aerial vehicle for efficient omnidirectional flight," *Int. J. Robot. Res.*, vol. 39, nos. 10–11, pp. 1305–1325, 2020.

[23] F. Morbidi, D. Bicego, M. Ryll, and A. Franchi, "Energy-efficient trajectory generation for a hexarotor with dual-tilting propellers," in *Proc. IEEE/RSJ Int. Conf. Intell. Robots Syst. (IROS)*, 2018, pp. 6226–6232.

[24] M. Hamandi, F. Usai, Q. Sablé, N. Staub, M. Tognon, and A. Franchi, "Design of multirotor aerial vehicles: A taxonomy based on input allocation," *Int. J. Robot. Res.*, vol. 40, nos. 8–9, pp. 1015–1044, 2021.

[25] D. Lee, S. Hwang, C. Kim, S. J. Lee, and H. J. Kim, "Minimally actuated tiltrotor for perching and normal force exertion," in *Proc. IEEE/RSJ Int. Conf. Intell. Robots Syst. (IROS)*, 2023, pp. 5027–5033.

[26] J. Bak, Y. Moon, J. Kim, S. Mohan, T. Seo, and S. Jin, "Hovering control of an underwater robot with tilting thrusters using the decomposition and compensation method based on a redundant actuation model," *Robot. Auton. Syst.*, vol. 150, 2022, Art. no. 103995.

[27] M. A. G. Rangel, A. Manzanilla, A. E. Z. Suarez, F. Muñoz, S. Salazar, and R. Lozano, "Adaptive non-singular terminal sliding mode control for an unmanned underwater vehicle: Real-time experiments," *Int. J. Control, Automat. Syst.*, vol. 18, pp. 615–628, 2020.

[28] R. D. Nussbaum, "Some remarks on a conjecture in parameter adaptive control," *Syst. Control Lett.*, vol. 3, no. 5, pp. 243–246, 1983.

[29] C. Chen, Z. Liu, Y. Zhang, C. L. P. Chen, and S. Xie, "Saturated Nussbaum function based approach for robotic systems with unknown actuator dynamics," *IEEE Trans. Cybern.*, vol. 46, no. 10, pp. 2311–2322, Oct. 2016.

[30] A. S. Morse, "Control using logic-based switching," in *Trends in Control: A European Perspective*, 1997, pp. 69–113.

[31] G. Cai, B. M. Chen, and T. H. Lee, *Unmanned Rotorcraft Systems*. Springer-Verlag, 2011.

[32] T. I. Fossen, *Handbook of Marine Craft Hydrodynamics and Motion Control*. Hoboken, NJ, USA: Wiley, 2011.

[33] D. Huang et al., "First principle modeling of a morphable unmanned aerial–aquatic vehicle: Mirs-Alioth," in *Proc. IEEE 18th Int. Conf. Control Automat. (ICCA)*, 2024, pp. 540–545.

[34] A. Healey and D. Lienard, "Multivariable sliding mode control for autonomous diving and steering of unmanned underwater vehicles," *IEEE J. Ocean. Eng.*, vol. 18, no. 3, pp. 327–339, Jul. 1993.

[35] L. Meier, D. Honegger, and M. Pollefeys, "PX4: A node-based multithreaded open source robotics framework for deeply embedded platforms," in *Proc. IEEE Int. Conf. Robot. Automat. (ICRA)*, 2015, pp. 6235–6240.

[36] C. Zhao and S. Yuan, "On tracking and antidisturbance ability of PID controllers," *SIAM J. Control Optim.*, vol. 62, no. 3, pp. 1857–1883, 2024.

[37] S. S. Ge, F. Hong, and T. H. Lee, "Adaptive neural control of nonlinear time-delay systems with unknown virtual control coefficients," *IEEE Trans. Syst., Man, and Cybern., Part B (Cybern.)*, vol. 34, no. 1, pp. 499–516, Feb. 2004.

[38] H. K. Khalil, "Universal integral controllers for minimum-phase nonlinear systems," *IEEE Trans. Autom. Control*, vol. 45, no. 3, pp. 490–494, Mar. 2000.

[39] E. Potokar, S. Ashford, M. Kaess, and J. G. Mangelson, "HoloOcean: An underwater robotics simulator," in *Proc. Int. Conf. Robot. Automat. (ICRA)*, 2022, pp. 3040–3046.

[40] T. R. Player et al., "From concept to field tests: Accelerated development of multi-AUV missions using a high-fidelity faster-than-real-time simulator," in *Proc. IEEE Int. Conf. Robot. Automat. (ICRA)*, 2023, pp. 3102–3108.

Dongyue Huang (Graduate Student Member, IEEE) received the B.Eng. degree in mechanical engineering from Queen's University Belfast, Belfast, U.K., and Guangdong University of Technology, Guangzhou, China, in 2019, and the M.Sc. degree in mechanical and automation engineering from The Chinese University of Hong Kong (CUHK), Shatin, N.T., Hong Kong, in 2020, where he is currently working toward the Ph.D. degree in mechanical and automation engineering, CUHK.

His research interests include design and control of unmanned multimodal vehicles.

Minghao Dou received the bachelor's degree in process equipment and control engineering from Dalian University of Technology, Dalian, China, in 2019. He is currently working toward the Ph.D. degree in mechanical and automation engineering, The Chinese University of Hong Kong, Shatin, N.T., Hong Kong.

His research interests include modeling and CFD simulation works of unmanned multimodal vehicles.

Xuchen Liu received the B.E. degree in mechanical engineering from Beihang University, Beijing, China, in 2018, and the M.Sc. degree in mechanical and automation engineering from The Chinese University of Hong Kong (CUHK), Shatin, N.T., Hong Kong, in 2020, where he is currently working toward the Ph.D. degree in mechanical and automation engineering, CUHK.

His research interests include design and control of unmanned multimodal vehicles.

Xinyi Wang received the bachelor's degree in flight vehicle design and engineering from Xiamen University, Xiamen, China, in 2019, and the Ph.D. degree in mechanical and automation engineering from The Chinese University of Hong Kong, Shatin, N.T., Hong Kong, in 2023.

She served as a Postdoctoral Researcher at the Hong Kong Centre for Logistics Robotics, Shatin, N.T., Hong Kong. Currently, she is a Postdoctoral Researcher in the Distributed Autonomous Systems and Control Lab at the University of Michigan, Ann Arbor, MI, USA. Her research interests include risk-aware multi-agent systems, optimization and control theory.

Chenggang Wang received the B.E. degree from Shandong University, Jinan, China, in 2017, and the Ph.D. degree from Shanghai Jiao Tong University, Shanghai, China, in 2023, both in control science and engineering.

Currently, he is a Postdoctoral Fellow with the Department of Automation, Shanghai Jiao Tong University, Shanghai, China. From 2022 to 2023, he was a Research Assistant with the Department of Mechanical and Automation Engineering, The Chinese University of Hong Kong, Shatin, N.T., Hong Kong, China. His research interests include control theory, underwater robotics, and optimization.

Ben M. Chen (Fellow, IEEE) received the B.S. degree in mathematics and computer science from Xiamen University, Xiamen, China, the M.S. degree in electrical engineering from Gonzaga University, Spokane, WA, USA, and the Ph.D. degree in electrical and computer engineering from Washington State University, Pullman, WA, USA, in 1983, 1988, and 1991, respectively. He is currently a Professor of mechanical and automation engineering with The Chinese University of Hong Kong (CUHK), Shatin, N.T., Hong Kong. Before joining CUHK in 2018, he was a Provost's Chair Professor with the Department of Electrical and Computer Engineering, National University of Singapore, Singapore, where he had worked for 25 years. He was an Assistant Professor with the Department of Electrical Engineering, State University of New York, Stony Brook, NY, USA, from 1992 to 1993, and a Software Engineer with the South China Computer Corporation, Guangzhou, China, from 1983 to 1986. His research interests include the development unmanned systems technologies and their applications.

Dr. Chen is a fellow of Academy of Engineering, Singapore. He has authored/co-authored hundreds of journal and conference articles, and ten research monographs in control theory and applications, unmanned systems and financial market modeling. He had served on the editorial boards of a dozen international journals including *Automatica* and IEEE TRANSACTIONS ON AUTOMATIC CONTROL. He currently serves as an Editor-in-Chief of *Unmanned Systems*, and an Editor of *International Journal of Robust and Nonlinear Control*.